UC Davis

UC Davis Previously Published Works

Title

Effect of different transport observations on inverse modeling results: case study of a long-term groundwater tracer test monitored at high resolution

Permalink

https://escholarship.org/uc/item/4n12j3gs

Journal

Hydrogeology Journal, 21(7)

ISSN

1431-2174

Authors

Rasa, Ehsan
Foglia, Laura
Mackay, Douglas M
et al.

Publication Date

2013-11-01

DOI

10.1007/s10040-013-1026-8

Peer reviewed

eScholarship.org Powered by the California Digital Library
University of California

NIH Public Access
Author Manuscript
Hydrogeol J. Author manuscript; available in PMC 2014 March 24.

Published in final edited form as:
Hydrogeol J. 2013 November ; 21(7): 1539–1554. doi:10.1007/s10040-013-1026-8.

Effect of different transport observations on inverse modeling results: case study of a long-term groundwater tracer test monitored at high resolution

Ehsan Rasa
Department of Civil and Environmental Engineering, University of California-Davis, One Shields Avenue, Davis, CA 95616, USA

Laura Foglia, **Douglas M. Mackay**, and **Kate M. Scow**
Department of Land, Air, and Water Resources, University of California-Davis, One Shields Avenue, Davis, CA 95616, USA

Abstract

Conservative tracer experiments can provide information useful for characterizing various subsurface transport properties. This study examines the effectiveness of three different types of transport observations for sensitivity analysis and parameter estimation of a three-dimensional site-specific groundwater flow and transport model: conservative tracer breakthrough curves (BTCs), first temporal moments of BTCs (m_1), and tracer cumulative mass discharge (M_d) through control planes combined with hydraulic head observations (h). High-resolution data obtained from a 410-day controlled field experiment at Vandenberg Air Force Base, California (USA), have been used. In this experiment, bromide was injected to create two adjacent plumes monitored at six different transects (perpendicular to groundwater flow) with a total of 162 monitoring wells. A total of 133 different observations of transient hydraulic head, 1,158 of BTC concentration, 23 of first moment, and 36 of mass discharge were used for sensitivity analysis and parameter estimation of nine flow and transport parameters. The importance of each group of transport observations in estimating these parameters was evaluated using sensitivity analysis, and five out of nine parameters were calibrated against these data. Results showed the advantages of using temporal moment of conservative tracer BTCs and mass discharge as observations for inverse modeling.

Keywords

Inverse modeling; Mass discharge; Tracer tests; Temporal moment of breakthrough curve; USA

Introduction

Computer models are widely used to simulate groundwater flow and reactive transport of contaminants in remediation system design. Inverse modeling and associated sensitivity analysis are helpful in efficiently estimating the values of multiple parameters

© Springer-Verlag Berlin Heidelberg 2013

erasa@ucdavis.edu Tel.: +1-530-5748193.
lfoglia@ucdavis.edu
dmmackay@ucdavis.edu
kmscow@ucdavis.edu
Present Address: E. Rasa Geosyntec Consultants, 1111 Broadway, 6th floor, Oakland, CA 94607, USA
Present Address: L. Foglia Institute of Applied Geosciences, Technical University Darmstadt, 64287, Darmstadt, Germany

NIH-PA Author Manuscript
NIH-PA Author Manuscript
NIH-PA Author Manuscript

NIH-PA Author Manuscript

NIH-PA Author Manuscript

NIH-PA Author Manuscript

simultaneously and evaluating data shortcomings (Poeter and Hill 1997). Inverse modeling has been used for decision making in groundwater management (Tiedeman and Gorelick 1993; Ulrich and Edwards 2003), groundwater flow calibration (Anderman et al. 1996; Foglia et al. 2007; Rittmann and McCarty 2001; Yager 2004), groundwater age problems (Ginn et al. 2009; Lovley et al. 1995), and groundwater transport problems (Bekins et al. 1999; Edwards and Grbić-Galić 1994; Essaid et al. 2003).

Conservative tracer experiments have been used to study flow and transport at both relatively homogenous sites in the USA—for example, Vandenberg Air Force Base, California (Mackay et al. 2012), Borden, Ontario (Mackay et al. 1986), and Cape Cod, Massachusetts (Leblanc et al. 1991)—and heterogeneous sites such as, the Macrodispersion Experiment (MADE) site in Columbus, Mississippi (Barlebo et al. 2004). To characterize the subsurface flow and transport parameters, several types of information derived from tracer experiments have been shown to be useful. These include travel-time distribution at transects perpendicular to the mean groundwater flow direction (Christensen et al. 2000; Cozzarelli et al. 2010; Lovley and Lonergan 1990; Rabus et al. 1993; Ruiz-Aguilar et al. 2002), travel time based on peak concentration (Cozzarelli et al. 2010; Lovley and Lonergan 1990), groundwater-flow velocity (Chen et al. 2008; Vanderborght et al. 2005), temporal moments of breakthrough curves BTC; (Barth and Hill 2005a, b; Mehl and Hill 2001), and mass discharge (Englert et al. 2009; Harvey and Gorelick 1995). Harvey and Gorelick (1995) used time values at which different portions of total mass passed a sampler (arrival time quantile) as observations to estimate the spatial pattern of aquifer hydraulic conductivity of a hypothetical aquifer. Harvey and Gorelick's (1995) results showed that using quantiles for arrival time, rather than concentrations, is more efficient for estimation procedures, since it provides a single quantile to represent the critical information contained in a breakthrough curve constructed from many concentration measurements. Barth and Hill (2005a, b) used temporal moments of conservative tracer breakthrough curves as observations and found that these provide a robust form of observation for a transport problem, since parameter sensitivities are less susceptible to variability associated with numerical errors. Mehl and Hill (2001) used data from a conservative tracer experiment in a heterogeneous sand tank to develop a two-dimensional (2D) model. They reported that the choice of solution techniques can significantly influence the estimated values of hydraulic conductivity owing to the error and numerical dispersion associated with each method. They also reported that different solution techniques demonstrated little difference in sensitivity analysis results. Different types of transport observations can have different effects on different sensitivity analysis and parameter estimation results, which none of the aforementioned studies have examined. In this study, data from a long-term tracer test were used to explore this using a simplified three-dimensional (3D) flow and transport model.

In this study, used data from a conservative tracer experiment at a research site at Vandenberg Air Force Base (VAFB), California, were used to construct and calibrate a 3D groundwater flow and transport model. The experiment provided high-quality tracer data from a high-resolution network of monitoring wells. The breakthrough curve (BTC) concentration data and hydraulic head values were measured frequently during the experiment at six transects downgradient of the injection source and perpendicular to groundwater flow direction. The effect of different types of transport observations (i.e., breakthrough concentrations, temporal moment of breakthrough curves, and cumulative mass discharge of a conservative tracer) on sensitivity analyses and parameter estimation results was assessed. Calibrated model results were evaluated based on differences between simulated and observed breakthrough curves and resulting plume shapes.

NIH-PA Author Manuscript

NIH-PA Author Manuscript

NIH-PA Author Manuscript

Background of research site

The experimental site at VAFB includes the area at and downgradient of a former fuel service station. A gasoline leak was found in 1994 at the station, and, in 1995, tanks and piping were excavated and backfilled with relatively permeable media (Fig. 1). Because many details on the characteristics of the site have already been discussed (Mackay et al. 2006; Wilson et al. 2002), only relevant details are repeated here. Figure 1 presents boundaries of the 1995 excavation of leaking underground storage tanks and piping, the network of monitoring wells (E-series transects oriented cross-gradient and the background wells), and the location of the in situ aerobic biobarrier installed by VAFB. Downgradient of the backfill, several thin, horizontal, sandy layers exist within 8 m of the ground surface. Figure 2 is the cross-sectional view that represents the conceptual model of the subsurface at the site based on the prior site characterization. The S3 sand layer is the main pathway for groundwater flow and thus contaminant migration from the depth interval impacted by the former spill. The S2 sand layer is less permeable and does not extend beyond the road. The S4 sand layer is not reached by the excavation based on the available knowledge. Therefore, the S3 sand layer is assumed to be the primary advective pathway in the numerical model reported here.

Tracer test experiment

As illustrated in Fig. 1, the experimental area was approximately 20 m wide and 70 m long (1,400 m^2); experimental details are reported in Mackay et al. (2012). In brief, groundwater was extracted (400 ml/min) from two of the background wells (locations shown in Fig. 1) and the combined flows spiked at a much lower rate with concentrated bromide solution. The total rate of bromide injection averaged about 122 g/d but varied throughout the period despite frequent adjustments. The amount of bromide mass spiked was measured nearly every day, allowing the resolution in Fig. 3 which shows the measured bromide mass injection rate of the bromide tracer throughout the experiment. Spiked groundwater was split into six individual injection wells in the EAA transect (wells EAA 4, 5, and 6 to create a plume in lane A and wells EAA 11, 12, and 13 to create lane B; see Fig. 1). The injection of groundwater containing bromide began on 11 July 2005 and continued for 299 days, ending 6 May 2006. Groundwater extraction and injection was continued (but without the bromide spike) for an additional 110 days, ending 24 August 2006. A total of 162 monitoring wells in 5 different transects (control planes) perpendicular to the direction of groundwater flow were used to sample the groundwater aquifer at the time of this experiment (Fig. 1). Possible inequalities in splitting by the injection system were ignored in this study and it was assumed that injection flowrate was the same for lanes A and B (200 ml/min) and that all six injection wells had equal bromide mass injection rates.

Injected tracer was monitored at six different transects and a total of 162 monitoring wells. These monitoring well transects are labeled EA, EB, EC, ED, EH, EJ and EJP in Fig. 1. Their distances from the injection wells (located in the EAA transect) are 1.7, 3.9, 7.8, 11.4, 35.3, and 44.9 m, respectively. Throughout the course of the tracer experiment, the plume was monitored by 12 snapshot samplings. Duplicate samples were collected during sampling and analysis of samples was conducted by ion chromatography at UC Davis (Mackay et al. 2012). Only a fraction of the duplicates were analyzed; when duplicate results were available, the average was used in this analysis. Before, during, and after the tracer injection, groundwater elevations at the site were monitored using standard methods.

NIH-PA Author Manuscript

NIH-PA Author Manuscript

NIH-PA Author Manuscript

Methods

Flow and transport model

The 3D conceptual model of the site consists of a laterally continuous uniform aquifer confined between two laterally continuous relatively less permeable aquitards (Fig. 2). Processes accounted for included transport, dispersion, and diffusion of the tracer (assumed nonreactive). The previous gasoline spill and other experiments at the site were assumed to have no impact on conservative solute transport during this experiment. Different values for porosity and hydraulic conductivity were assumed for the aquifer, aquitard layers, and backfilled excavation zones, based on site-specific analyses or literature (Table 1). The hydraulic gradient, as estimated based on groundwater elevation monitoring, was 0.0132 with a 95 % confidence interval of 0.0004 (Mackay et al. 2012). Constant head boundary condition (based on head measurements) was used at the upstream and downstream limit of the study area. Other than two extraction wells and the six injection wells mentioned (Fig. 1), EJP wells were intermittently pumped, creating a minor increase in the velocity of the groundwater flowing through the upgradient EJ transect. All 23 EJP wells were pumped occasionally with a low extraction rate of 0.06 L/min for a separate field experiment. The date and duration of EJP pumping events are described in Mackay et al. (2012). All groundwater extraction and pumping events are included in this modeling study to better represent the flow regime at the site. Recharge was assumed to be negligible in the modeled area during the experimental period.

MODFLOW-2000 (Harbaugh et al. 2000) with preconditioned conjugate-gradient 2 (PCG2) (Hill 1990) was used to simulate the transient flow regime and head values. To simulate the transport, MT3DMS (Zheng 2010) was used. A third-order total-variation-diminishing (TVD) scheme (Harten 1983, 1997) was used to solve the advection term, while the implicit general conjugate-gradient (GCG) was used to solve the dispersion and sink/source term. The model grid was oriented so that the groundwater flow direction was aligned with the model rows. The model area was 120 m in the direction of groundwater flow (X direction), 60 m in the direction perpendicular to it (Y direction), with the top 6 m of the subsurface considered (Z direction). The 3D finite difference grid consists of 130 rows, 230 columns, and 36 layers and was more refined around the plume area (0.36 m×0.18 m×0.10 m in X, Y, and Z directions, respectively).

The grid Peclet number and Courant number (Eqs. 1 and 2) were checked to ensure convergence and stability of the transport model.

$$\mathrm{Pe}=\frac{V.\Delta x}{D} \quad (1)$$

$$\mathrm{Cr}=\frac{V.\Delta t}{\Delta x} \quad (2)$$

where Pe is the grid Peclet stability number, V is the average flow velocity (L T^{-1}), Δx is the grid spacing in the direction of groundwater flow (L), D is the hydrodynamic dispersion coefficient (L^2 T^{-1}, and Cr is the Courant stability number. The grid Peclet number is a measure of the level of oscillation (Batu 2006). While it is usually suggested to select the grid spacing so that the Peclet number does not exceed 2, in many cases acceptable solutions with mild oscillation are achieved with grid Peclet numbers as high as 10 (Huyakorn and Pinder 1983). A TVD solution scheme was shown to achieve satisfactory and mass conservative solutions at grid Peclet numbers of 5 and 14 (Zheng and Wang 1999). The Courant number controls the oscillation of the numerical solution owing to temporal

NIH-PA Author Manuscript

NIH-PA Author Manuscript

NIH-PA Author Manuscript

discretization, and it needs to be below 1 (Daus and Frind 1985). In this study, the grid spacing was made sufficiently fine to keep the Peclet number low (varying between 0.36 and 3.6, depending on the value of dispersivity), and time discretization in the solution was such that the Courant number was always below 1.

Inverse model

The US Geological Survey (USGS) universal inverse modeling code, UCODE_2005 (Poeter et al. 2005) was used to perform sensitivity analysis and parameter estimation. Sensitivity analysis and calibration methods allow the modeler to explore the relations between different types of data and the processes represented in the model, including the testing of hypotheses about system structure.

The sensitivity analysis applied for this paper is suggested by Hill and Tiedeman (2007), and includes computationally frugal local, or gradient, methods. Local sensitivity analysis methods use the sensitivities (derivatives) of simulated values with respect to parameters, and the sensitivities are evaluated at a specific set of parameter values. Statistics calculated with sensitivity analysis provide useful and immediate information about the importance of different observations, processes and parameters in the system design. Similar to the method described in Hill and Tiedeman (2007), the objective function shown in Eq. 3 was used in this study to perform least-squares-based calibration of the groundwater model:

$$S\left(\bar{b}\right)=\sum_{\mathrm{i}=1}^{\mathrm{nh}}\omega_{\mathrm{i}}\left(h_i-h_{\mathrm{i}}^{'}\right)^2+\sum_{\mathrm{j}=1}^{\mathrm{nc}}\omega_{\mathrm{j}}\left(C_{\mathrm{j}}-C_{\mathrm{j}}^{'}\right)^2+\sum_{\mathrm{k}=1}^{\mathrm{nm}_1}\omega_{\mathrm{k}}\left(m_{1\mathrm{k}}-m_{1_{\mathrm{k}}}^{'}\right)^2+\sum_{\mathrm{m}=1}^{\mathrm{nm}_d}\omega_{\mathrm{m}}\left(M_{\mathrm{dm}}-M_{\mathrm{d_m}}^{'}\right)^2 \quad (3)$$

where $S\left(\bar{b}\right)$ is the objective function value, b is the vector containing values of each of the np parameters being estimated, h, C, m_1, and M_{d} are the observed hydraulic head (L), BTC concentration (M L^{-3}), first temporal moment (T), and cumulative mass discharge (M) values, respectively; h', C', m'_1, and M'_{d} are the corresponding simulated values, nh, nc, nm_1, and nm_{d} are the number of hydraulic head, BTC concentration, first temporal moment, and mass discharge observations, respectively, and ω is the weight that corresponds to the observation and is based on statistics of the observation errors.

Fit independent statistics have first been used here to evaluate sensitivity of the system to parameters and observations. They include: dimensionless scaled sensitivity (DSS), composite scaled sensitivity (CSS), and parameter correlation coefficient (PCC):

$$\mathrm{DSS}_{\mathrm{ij}}=\left(\frac{\partial y_{\mathrm{i}}^{'}}{\partial b_{\mathrm{j}}}\right)\Bigg|_{\mathrm{b}}|b_j|\omega_{\mathrm{ii}}^{\frac{1}{2}} \quad (4)$$

$$\mathrm{DSS}_{\mathrm{j}}=\left(\sum_{\mathrm{i}=1}^{n_{\mathrm{obs}}}(\mathrm{DSS}_{\mathrm{ij}})^2|_{\mathrm{bj}}/n_{\mathrm{obs}}\right)^{\frac{1}{2}} \quad (5)$$

$$\mathrm{PCC}_{\mathrm{jk}}=\frac{\mathrm{cov}(b)_{\mathrm{jk}}}{\left(\mathrm{var}(b)_{\mathrm{jj}}.\mathrm{var}(b)_{\mathrm{kk}}\right)} \quad (6)$$

where y_{i}' is the simulated value corresponding to the ith observation (y_{i}), b_{j} is the jth parameter, n_{obs} is the number of observations, cov $(b)_{\mathrm{jk}}$ is the covariance between jth and kth parameters and var$(b)_{\mathrm{jj}}$ and var$(b)_{\mathrm{kk}}$ are the variances of each of the jth and kth

NIH-PA Author Manuscript

NIH-PA Author Manuscript

NIH-PA Author Manuscript

parameters (Hill and Tiedeman 2007). DSS is used to evaluate the importance of an individual observation in the estimation of each parameter, while CSS indicates the importance of observations as a whole to a single parameter, compared with the accuracy on the observation (Barth and Hill 2005a). A larger DSS indicates greater importance of the observation relative to its error, and a large CSS value indicates a parameter for which more information is provided by all observations. PCC is calculated for each possible pair of the model parameters in UCODE_2005. It indicates whether there is a unique parameter estimation result for each pair, given the observation and model. Usually when all PCC values are less than 0.95, it is assumed that parameter values can be estimated uniquely (Hill and Tiedeman 2007). Parameter sensitivity and correlation results were used to design a productive regression and identify important observations.

Observations and weighting method

Four categories of observations were used in this study: hydraulic head, BTC concentrations, temporal first moments of BTCs, and tracer mass discharge through transects (Table 2). Throughout the experiment, hydraulic head was measured at the S3 aquifer and tracer concentration was measured at six monitoring well transects with full aquifer screens (Fig. 1). A total of 133 hydraulic head values and 1,158 concentrations were selected as observations.

The temporal first moment of the breakthrough curve is representative of the arrival time of the center of the mass (thus, it is different from the travel time); it is defined using Eq. (7). Groundwater sampling at three transects (ED, EH, and EJ) started earlier and was conducted more frequently than for transects EA, EB, and EC. Therefore, breakthrough curves from wells located in transects ED, EH, and EJ were used to calculate the observed values of temporal first moments. Monitoring wells that were completely outside the two bromide lanes were not included in the first moment calculations, since the breakthrough curves at those wells were relatively noisy and would have a misleading value of first moments. A total of 23 values of temporal first moments were selected as observations.

$$m_1 = \frac{\int t.c(t)\ dt}{\int c(t)\ dt} \quad (7)$$

The amount of bromide mass discharged through a well transect (control plane) orthogonal to the direction of groundwater flow was calculated using concentration measurements at full screen thickness monitoring wells. A commonly used form of the Thiessen Polygon Method (TPM) for calculating mass discharge through a control plane is presented in Eq. (8):

$$m_{\mathrm{d}} = \sum_{n_{mw}} C.K.i.A \quad (8)$$

where n_{mw} is the number of sampling segments in the control plane, C is the concentration of the solute in discrete samples (M L^{-3}), K is the aquifer hydraulic conductivity (L T^{-1}), i is the groundwater hydraulic gradient at the control plane, and A is the area of the aquifer associated to each sampling point (L^2). As mentioned, more refined BTC data were available at three transects of ED, EH, and EJ, which made it possible to calculate mass discharge values at 12 time points throughout the experiment (Mackay et al. 2012). These 36 values of mass discharge were used in the inverse model as the fourth group of model observations.

NIH-PA Author Manuscript

NIH-PA Author Manuscript

NIH-PA Author Manuscript

Objective functions such as that shown in Eq. (3) are usually weighted to account for different units, measurement uncertainty, and precision of different observations contributing to the objective function. Generally, precise determination of observation weights is not possible because the information available on observation errors is not sufficient; rather, the aim is usually to limit the weights so that sensitivity analysis results and parameter calibration are consistent (Foglia et al. 2009). In this study, different weighting methods for different groups of observations were applied. Hydraulic head observations at monitoring wells ranged from 8.6 to 9.6 m above mean sea level (Table 2). In all, 1 % of the entire head loss in the model (the upper boundary minus the lower boundary condition: 1.6 m) was used as the standard deviation of simulated head values and was applied uniformly to all of the head observations. Tracer BTCs at the monitoring wells were in a wider range of 0–350 mg/L; therefore, it is reasonable to apply weights that are functions of observation values (e.g., coefficient of variation; Hill and Tiedeman 2007). To weight the tracer BTCs, a coefficient of variation of 10 % was applied to observations that were larger than 31 mg/L. For observations that were smaller than 31 mg/L, a standard deviation of 3.1 mg/L (within the estimated background bromide concentration at the site during this experiment) was applied to the breakthrough concentration observations. The temporal first moment of breakthrough curve (m_1) and cumulative mass discharge (M_d) observations were calculated based on the concentration measurements; therefore, the uncertainties associated with these groups of observations were evaluated based on the error in concentration measurements. The standard deviation and coefficient of variation in concentration observations (Table 2) were used to create a normal probability function and generate 1,000 random populations. The m_1 and M_d values were then quantified for each of the 1,000 populations and the corresponding standard deviations were used to weight the first moment and cumulative mass discharge observations.

To examine the impact of different types of transport observations derived from a tracer injection experiment, sensitivities of the model parameters were evaluated using three approaches, each having a different combination of observations: (1) hydraulic head and BTC concentrations, (2) hydraulic head and temporal first moment of BTC, and (3) hydraulic head and mass discharge values. The sensitivity analysis and parameter correlation results in each approach were used to select a subset of parameters for parameter estimation.

Results

Sensitivity analysis

Sensitivity of all model parameters (listed in Figs. 4 and 5) with respect to observations was evaluated using UCODE_2005. To compare the effects of different transport observations (BTC, m_1, and M_d) sensitivity analysis was performed for the three approaches described above using the same initial parameter value (Table 1). Figure 4 shows the comparison between the sensitivity of model parameters to individual observations using the DSS plots (Fig. 4), while parameter sensitivity to observations as a whole was assessed using the CSS measure (Fig. 5).

When hydraulic head measurements and transient tracer concentrations were used as observations (approach 1), hydraulic conductivity and porosity of the aquifer had the highest CSS value and were the most sensitive parameters. Longitudinal and transverse horizontal dispersivities were the most sensitive among the other parameters. Effective diffusion coefficient and aquitard hydraulic conductivity were the least sensitive parameters. Figure 4 shows how different observations impact the sensitivity of each parameter. Each cell in Fig. 4 represents an observation data point in either space or time. In the first approach, BTC from transects closer to the injection wells (EA–ED) had more contribution to sensitivity of aquifer hydraulic conductivity and dispersivity compared with wells further downgradient

NIH-PA Author Manuscript

NIH-PA Author Manuscript

NIH-PA Author Manuscript

(EH and EJ; Fig. 4a). Figure 4a shows that there are two distinguishable DSS levels detected for EA wells. This is perhaps because injection was performed in two different lanes (lane A and lane B, as shown in Fig. 1); BTC data from wells that were located within the plumes had higher DSS values than data from the wells that were outside the plume. For transects that are further downgradient (EJ), the two injection lanes are laterally dispersed and cover a larger width; therefore, the difference between DSS values within each well transect is less obvious. Absolute PCC values very close to 1.0 indicate that observations do not provide enough information to estimate parameters uniquely (Hill and Tiedeman 2007). Absolute PCC values >0.90 are summarized in Table 3 for all three approaches.

As in approach 1, hydraulic conductivity and porosity of the aquifer were the most sensitive parameters and aquitard hydraulic conductivity, transverse horizontal dispersivity, and diffusion coefficient were the least sensitive parameter in approaches 2 and 3 (Fig. 5). Sensitivity of the model to transverse vertical dispersivity, effective diffusion coefficient, and aquitard porosity was higher (by a factor of 2–3) when m_1 or M_d observations were used instead of BTC. Figure 4b shows that first temporal moments of BTC from wells that are within the plume but further downgradient (EJ wells) were more important observations to estimate hydraulic conductivity and porosity of the aquifer (higher DSS) than the wells that are closer to the injection wells (e.g., ED, Fig. 4b); however, within each monitoring transect first moments show similar DSS. This is because the monitoring transects are perpendicular to the groundwater flow direction and slight changes in aquifer parameters during perturbation has similar effects on the first moments of the wells located on the same transect. Several high PCC values were reported by the model in the second approach (Table 3). Figure 4c shows that when cumulative mass discharge values through monitoring transects at different times were used as observations (approach 3), earlier monitoring of tracer arrival at well transects is more important in estimating the model parameters. Unlike approach 1, M_d observations from transects further downgradient had higher DSS values for longitudinal and transverse horizontal dispersivities.

Results of parameter correlation analysis (shown in Table 3) showed strong correlation between transverse vertical dispersivity, diffusion coefficient, and the aquifer and aquitard porosity parameters in approach 2. For example, PCC values between diffusion coefficient and aquifer porosity and between diffusion coefficient and aquitard porosity were 0.99 and −0.99, respectively. For approach 3, transverse horizontal dispersivity and transverse vertical dispersivity were highly correlated with longitudinal dispersivity, and diffusion coefficient had high correlation with aquitard porosity (Table 3).

The list of parameters to be calibrated (Table 4) was determined based on analyzing the sensitivity of the parameters (Figs. 4 and 5) and the parameter correlation coefficients (Table 3). Parameters with high correlations were kept constant during calibration and fixed to their initial values (listed in Table 1). For example, based on core sampling measurements and site characterization data, a fixed value of aquifer porosity at 0.35 was chosen.

Parameter estimation

Parameters were estimated using the three approaches discussed previously, and results are presented in Table 4. Model outputs with optimized parameters are compared to observed values and to results obtained with the other approaches in Figs. 6, 7, 8 and 10.

The calibrated aquifer hydraulic conductivity values for the three models were within a narrow range of 10.89–16.96 m/d, which is consistent with previous investigations at the site (Mackay et al. 2012). The estimated values of aquitard hydraulic conductivity and hydraulic conductivity of the backfill area for the three approaches varied over a wider range compared to estimated aquifer hydraulic conductivity (Table 4). The backfilled hydraulic

NIH-PA Author Manuscript

NIH-PA Author Manuscript

NIH-PA Author Manuscript

conductivity ($K_{x\text{-backfill}}$) value estimated using approach 1 was lower than that of the aquifer. Most of the investigations at the site have been focused on the aquifer characterization. Therefore there are no available data to reject the range of variability of aquitard hydraulic conductivity and hydraulic conductivity of the backfill area.

All three approaches resulted in longitudinal dispersivity values between 0.18 and 0.55 m, that is, within the values expected from examination of other analyses previously done at the site. The transverse horizontal dispersivity value estimated by the second approach was 0.02 times the corresponding longitudinal dispersivity value, which is within the expected range of this parameter based on the available knowledge from this site (e.g., Rasa et al. 2013).

Values of the simulated versus observed hydraulic heads for all three approaches are compared in Fig. 6, while Fig. 7 presents the simulated and field measured bromide breakthrough curves at four monitoring wells arbitrarily chosen from four different monitoring well transects at the site. While the three approaches resulted in relatively similar values of hydraulic heads, the second and the third approach reproduced the best fit to the maximum breakthrough concentration data, as shown in Fig. 7. This figure also indicates that the tracer arrival time was better represented for EC and ED transects, whereas the elution of the tracer was best reproduced by EH and EJ simulated results. Comparing the simulated and observed breakthrough curves for the three approaches indicated that the overall trend of the tracer was simulated by the model, although the maximum concentration at transects closer to the injection wells (EA–ED) was not matched. Values of observed versus simulated temporal first moments (approach 2) of breakthrough curves are compared in Fig. 8. The first moment of a breakthrough curve is representative of the arrival time of the center of mass of the tracer, based on Eq. 7. That is why the simulated values of first moments for monitoring wells located on the same transects are very close to each other. Based on the measured tracer concentrations, mass discharge values through ED, EH, and EJ transects were calculated. Figure 9 compares the values of simulated and observed mass discharge values (approach 3). For the first 300 days of injection, a good match was simulated by the model for mass discharge values through the ED, EH and EJ transects. The total cumulative mass discharged through EH and EJ after 460 days was slightly underestimated by the model. The model shows more tailing of the tracer than was observed in the EH and EJ transects (Fig. 9). As these transects are farther from the injection source than ED, it would be expected that tailing in the S3 aquifer would be more pronounced due to diffusion into and back out of the under- and over-lying silty and clayey silty aquitards. Thus, Fig. 9 indicates that model approach 3 overestimates the diffusive effects.

Discussion

Results of this case study provide the opportunity to examine the efficiency of calibrating a flow and transport model based on a given set of data from a tracer test (i.e., hydraulic head and tracer concentration). To evaluate the performance of the calibrated model in reproducing the plume behavior, the simulated concentrations at all 162 monitoring wells using calibrated approaches 1–3 were used to create plots of plume shapes. Figure 10a compares the observed plume shape and the three simulated plumes at 73 days. These simulated plumes represent the production of plumes from the two side-by-side injection lanes. Figure 10b,c compare the same plumes at 244 days (nearest to the maximum concentration at all monitoring wells) and 343 days (elution of plumes from the site), respectively. Comparison of the results shows that the plume shape and concentrations predicted by calibration approach 2 (where first temporal moments of breakthrough curves were used as the observation) are the closest to the plots of observed plume concentrations. The tailing of the plume and elution time were also well represented by the calibrated model when the second approach was used.

NIH-PA Author Manuscript

NIH-PA Author Manuscript

NIH-PA Author Manuscript

The possible reason why using the breakthrough curve moments was the most efficient in calibrating the model is presented here. When temporal first moment of the breakthrough curve was used, the calibration aimed to match the arrival time of the center of the mass at each monitoring location, providing better matches to breakthrough and elution time at each location. This has resulted in a generally better fit to the observed tracer concentration throughout the plume at different times (Fig. 10). Additionally, sensitivity analysis results calculated for temporal moments of BTCs are usually less sensitive to numerical errors in highly advective systems such as is the case in this study (Barth and Hill 2005b; Cirpka and Kitanidis 2000). Using BTC moments has another advantage in that they provide feedback to the model and remain sensitive even when the observed and simulated BTCs do not overlap (Barth and Hill 2005a).

The estimated value of $K_{\text{x-backfill}}$ was higher than that of the estimated $K_{\text{x-aquifer}}$ in approach 2. This is as expected, since the excavated area was backfilled with coarser material which is expected to have a higher hydraulic conductivity. Adding prior information on the $K_{\text{x-backfill}}$ parameter could help with better estimation of this parameter in approach 3. Also, adding prior information on transverse horizontal dispersivity can perhaps lower the parameter correlation coefficient between longitudinal dispersivity (α_L) and horizontal transverse dispersivity (α_T) in approach 1 and allow estimation of horizontal dispersivity. Prior information on dispersivity parameters was not available at the time of this study and, therefore, prior values have not been included in the regressions. Future work will take into account the effect of prior information on parameter estimation results (including reactive transport modeling parameters).

Appropriate weighting of different observation groups had a great impact on parameter estimation results in this study. Weights need to reflect the relative accuracy of the measurements. A better match to BTCs was observed when these observations were weighted as a percent of the observed value, which is expressed as coefficient of variation (Table 2; parameter estimation results using uniform weighting are not presented here). Overall, examining the available observations, associated measurement errors, determining more important observations, and choosing an effective weighting method showed to be a critical first step in this inverse modeling study.

Effective remediation and decision making at contaminated sites requires a good understanding of different properties of the aquifer. Non-reactive tracer tests are an excellent way to yield new information on the fate and transport of solutes. Results of tracer tests can be used to better characterize and estimate some of the unknown parameters such as hydraulic conductivity, porosity, and dispersivity. These estimated values can be used later in conceptual fate and transport models of reactive solutes and remediation designs. Using models calibrated against different sets of observations derived from the same set of field data allows the analysis of the different estimated parameter values and the comparison of the different model outcomes.

Conclusions

Results of model sensitivity analysis indicated the importance of choice of parameters on the modeling of transport of bromide downgradient of the injection wells. For the three calibration approaches where different transport observations were used (conservative tracer BTCs, temporal first moments of breakthrough curves, and mass discharge values were used as observations), hydraulic conductivity and porosity of the aquifer were the most sensitive parameters. Porosity value was fixed, based on the previous laboratory experiments of the cores taken from the site.

NIH-PA Author Manuscript

NIH-PA Author Manuscript

NIH-PA Author Manuscript

Using more integrated transport observations such as temporal first moment of breakthrough curves and mass discharge of conservative tracer, provided the best parameter estimation results. When the first moments were used as observations, BTC data and plume behavior were better reproduced than when breakthrough curve observations were used. BTC moments provide feedback to the model and remain sensitive even when the observed and simulated BTCs do not overlap or the peak concentrations are not similar. Examining the available observations, identifying the important observations and parameters using sensitivity analysis, and applying an effective weighting method that reflects the relative accuracy of the measurements were crucial steps of this inverse modeling study.

This study shows that assessing different model outputs (e.g., mass discharge over time, temporal moments, etc.) and efficiently calibrating them require different types of observations. If enough knowledge of the site and enough data are available, it is possible to derive observations (such as moments of breakthrough curve and tracer mass discharge through control planes) from a conservative tracer experiment to constrain the range of calibration parameters.

Acknowledgments

The American Petroleum Institute and Superfund Training Program of the National Institute of Environmental Health Sciences (Award Number P42ES004699) provided funding and support for this modeling study. The content is solely the responsibility of the authors and does not necessarily represent the official views of the National Institute of Environmental Health Sciences or the National Institutes of Health. Primary funding for the field experimental work was provided by a subcontract to UC Davis by Malcolm Pirnie, Inc., the primary contractor to the Environmental Security Technology Certification Program (ESTCP) for project ER-0318. We thank Phil Kaiser, Mada Velasco, Max Justice, Sunitha Gurusinghe, Mamie Inoue-Nozawa, and Sham Goyal for their parts in completing the field experiments, and Murray Einarson of Haley & Aldrich and Chin Man Mok of AMEC-Geomatrix for initial modeling and advice. We also thank Dr. Mary Hill and Prof. Steffen Mehl for reviewing this study and providing valuable feedback and Professor Tim Ginn for reviewing and contributions.

References

Anderman ER, Hill MC, Poeter EP. Two-dimensional advective transport in ground-water flow parameter estimation. Ground Water. 1996; 34(6):1001–1009.

Barlebo HC, Hill MC, Rosbjerg D. Investigating the Macrodispersion Experiment (MADE) site in Columbus, Mississippi, using a three-dimensional inverse flow and transport model. Water Resour Res. 2004; 40(4):W04211.

Barth GR, Hill MC. Numerical methods for improving sensitivity analysis and parameter estimation of virus transport simulated using sorptive-reactive processes. J Contam Hydrol. 2005a; 76(3–4):251–277. [PubMed: 15683883]

Barth GR, Hill MC. Parameter and observation importance in modelling virus transport in saturated porous media: investigations in a homogenous system. J Contam Hydrol. 2005b; 80(3–4):107–129. [PubMed: 16202474]

Batu, V. Applied flow and solute transport modeling in aquifers: fundamental principles and analytical and numerical methods. Taylor and Francis; Boca Raton, FL: 2006. p. 667

Bekins BA, Godsy EM, Warren E. Distribution of microbial physiologic types in an aquifer contaminated by crude oil. Microb Ecol. 1999; 37(4):263–275. [PubMed: 10341056]

Chen YD, Barker JF, Gui L. A strategy for aromatic hydrocarbon bioremediation under anaerobic conditions and the impacts of ethanol: a microcosm study. J Contam Hydrol. 2008; 96(1–4):17–31. [PubMed: 17964687]

Christensen TH, et al. Characterization of redox conditions in groundwater contaminant plumes. J Contam Hydrol. 2000; 45(3–4):165–241.

Cirpka OA, Kitanidis PK. Sensitivity of temporal moments calculated by the adjoint-state method and joint inversing of head and tracer data. Adv Water Resour. 2000; 24(1):89–103.

NIH-PA Author Manuscript

NIH-PA Author Manuscript

NIH-PA Author Manuscript

Cozzarelli IM, Bekins BA, Eganhouse RP, Warren E, Essaid HI. In situ measurements of volatile aromatic hydrocarbon biodegradation rates in groundwater. J Contam Hydrol. 2010; 111(1–4):48–64. [PubMed: 20060615]

Daus AD, Frind EO. An alternating direction Galerkin technique for simulation of contaminant transport in complex groundwater systems. Water Resour Res. 1985; 21(5):653–664.

Edwards EA, Grbić-Galić D. Anaerobic degradation of toluene and o-xylene by a methanogenic consortium. Appl Environ Microbiol. 1994; 60(1):313–322. [PubMed: 8117084]

Englert A, Hubbard SS, Williams KH, Li L, Steefel CI. Feedbacks between hydrological heterogeneity and bioremediation induced biogeochemical transformations. Environ Sci Technol. 2009; 43(14): 5197–5204. [PubMed: 19708341]

Essaid HI, et al. Inverse modeling of BTEX dissolution and biodegradation at the Bemidji, MN crude-oil spill site. J Contam Hydrol. 2003; 67(1–4):269–299. [PubMed: 14607480]

Foglia L, Mehl SW, Hill MC, Perona P, Burlando P. Testing alternative ground water models using cross-validation and other methods. Ground Water. 2007; 45(5):627–641. [PubMed: 17760588]

Foglia L, Hill MC, Mehl SW, Burlando P. Sensitivity analysis, calibration, and testing of a distributed hydrological model using error-based weighting and one objective function. Water Resour Res. 2009; 45:W06427.

Ginn TR, Haeri H, Massoudieh A, Foglia L. Notes on groundwater age in forward and inverse modeling. Transport Porous Media. 2009; 79(1):117–134.

Harbaugh, AW.; Banta, ER.; Hill, MC.; McDonald, MG. US Geol Surv Open-File Rep. 2000. MODFLOW-2000, the U.S. Geological Survey modular groundwater model: user guide to modularization concepts and the ground-water flow process; p. 00-92.

Harten A. High-resolution schemes for hyperbolic conservation-laws. J Comput Phys. 1983; 49(3): 357–393.

Harten A. High resolution schemes for hyperbolic conservation laws (Reprinted from the *Journal of Computational Physics*, vol 49, pg 357-393, 1983). J Comput Phys. 1997; 135(2):260–278.

Harvey CF, Gorelick SM. Mapping hydraulic conductivity: sequential conditioning with measurements of solute arrival time, hydraulic-head, and local conductivity. Water Resour Res. 1995; 31(7):1615–1626.

Hill, MC. US Geol Surv Water-Resour Invest Rep. 1990. Preconditioned conjugate-gradient 2 (PCG2), a computer program for solving ground-water flow equations; p. 90-4048.

Hill, MC.; Tiedeman, CR. Effective groundwater model calibration: With analysis of data, sensitivities, predictions, and uncertainty. Wiley, Hoboken; NJ: 2007.

Huyakorn, PS.; Pinder, GF. Computational methods in subsurface flow. Academic; New York: 1983. p. 473

Leblanc DR, et al. Large-scale natural gradient tracer test in sand and gravel, Cape-Cod, Massachusetts: 1. experimental-design and observed tracer movement. Water Resour Res. 1991; 27(5):895–910.

Lovley DR, Lonergan DJ. Anaerobic oxidation of toluene, phenol, and p-cresol by the dissimilatory iron-reducing organism, GS-15. Appl Environ Microbiol. 1990; 56(6):1858–1864. [PubMed: 16348226]

Lovley DR, Coates JD, Woodward JC, Phillips E. Benzene oxidation coupled to sulfate reduction. Appl Environ Microbiol. 1995; 61(3):953–958. [PubMed: 16534979]

Mackay DM, et al. Impact of ethanol on the natural attenuation of benzene, toluene, and o-xylene in a normally sulfate-reducing aquifer. Environ Sci Technol. 2006; 40(19):6123–6130. [PubMed: 17051810]

Mackay DM, et al. Mass discharge in a tracer plume: evaluation of the Theissen polygon method. Ground Water. 2012; 50(6):895–907. [PubMed: 22324777]

Mackay DM, Freyberg DL, Roberts PV, Cherry JA. A natural gradient experiment on solute transport in a sand aquifer: 1. approach and overview of plume movement. Water Resour Res. 1986; 22(13): 2017–2029.

Mehl S, Hill MC. A comparison of solute-transport solution techniques and their effect on sensitivity analysis and inverse modeling results. Ground Water. 2001; 39(2):300–307. [PubMed: 11286078]

NIH-PA Author Manuscript

NIH-PA Author Manuscript

NIH-PA Author Manuscript

Mirkin MV, Arca M, Bard AJ. Scanning electrochemical microscopy. 22. Examination of thin solid films of Agbr: ion diffusion in the film and heterogeneous kinetics at the film solution interface. J Phys Chem. 1993; 97(41):10790–10795.

Parker BL, Cherry JA, Chapman SW. Field study of TCE diffusion profiles below DNAPL to assess aquitard integrity. J Contam Hydrol. 2004; 74(1–4):197–230. [PubMed: 15358493]

Patil SF, Adhyapak NG, Joshi SS. Diffusion of bromide, iodide and thallium ions at various temperatures. Appl Radiat Isot. 1986; 37(1):37–39.

Poeter EP, Hill MC. Inverse models: a necessary next step in ground-water modeling. Ground Water. 1997; 35(2):250–260.

Poeter, EP.; Hill, MC.; Banta, ER.; Mehl, S.; Christensen, S. US Geol Surv Tech Methods. 2005. UCODE_2005 and six other computer codes for universal sensitivity analysis, calibration, and uncertainty evaluation; p. 6-A11.

Rabus R, Nordhaus R, Ludwig W, Widdel F. Complete oxidation of toluene under strictly anoxic conditions by a new sulfate-reducing bacterium. Appl Environ Microbiol. 1993; 59(5):1444–1451. [PubMed: 7686000]

Rasa E, Chapman SW, Bekins BA, Fogg GE, Scow KM, Mackay DM. Role of back diffusion and biodegradation reactions in sustaining an MTBE/TBA plume in alluvial media. J Contam Hydrol. 2011; 126(3–4):235–247. [PubMed: 22115089]

Rasa E, Bekins BA, Mackay DM, de Sieyes NR, Wilson JT, Feris KP, Wood IA, Scow KM. Impacts of ethanol-blended fuel release on groundwater and fate of produced methane: simulation of field observations. Water Resour Res. 2013 doi:10.1002/wrcr.20382.

Rittmann, BE.; McCarty, PL. McGraw-Hill Series in Water Resources and Environmental Engineering. McGraw-Hill; Boston, MA: 2001. Environmental biotechnology: principles and applications; p. 754

Ruiz-Aguilar GML, Fernandez-Sanchez JM, Kane SR, Kim D, Alvarez PJJ. Effect of ethanol and methyl-Tert-butyl ether on monoaromatic hydrocarbon biodegradation: response variability for different aquifer materials under various electron-accepting conditions. Environ Toxicol Chem. 2002; 21(12):2631–2639. [PubMed: 12463558]

Tiedeman C, Gorelick SM. Analysis of uncertainty in optimal groundwater contaminant capture design. Water Resour Res. 1993; 29(7):2139–2153.

Ulrich AC, Edwards EA. Physiological and molecular characterization of anaerobic benzene-degrading mixed cultures. Environ Microbiol. 2003; 5(2):92–102. [PubMed: 12558592]

Vanderborght J, Kemna A, Hardelauf H, Vereecken H. Potential of electrical resistivity tomography to infer aquifer transport characteristics from tracer studies: a synthetic case study. Water Resour Res. 2005; 41(6):W06013.

Wilson RD, Mackay DM, Scow KM. In situ MTBE biodegradation supported by diffusive oxygen release. Environ Sci Technol. 2002; 36(2):190–199. [PubMed: 11827053]

Yager RM. Effects of model sensitivity and nonlinearity on nonlinear regression of ground water flow. Ground Water. 2004; 42(3):390–400. [PubMed: 15161156]

Zheng, C. Technical Report to the US Army Engineer Research and Development Center, Department of Geological Sciences. University of Alabama; Birmingham, AB: 2010. MT3DMS v5.3 supplemental user's guide; p. 51

Zheng, C.; Wang, PP. MT3DMS, a modular three-dimensional multi-species transport model for simulation of advection, dispersion and chemical reactions of contaminants in ground-water systems: documentation and users guide. Contract report SERDP-99-1, US Army Engineer Research and Development Center; Vicksburg, MI: 1999.

NIH-PA Author Manuscript

NIH-PA Author Manuscript

NIH-PA Author Manuscript

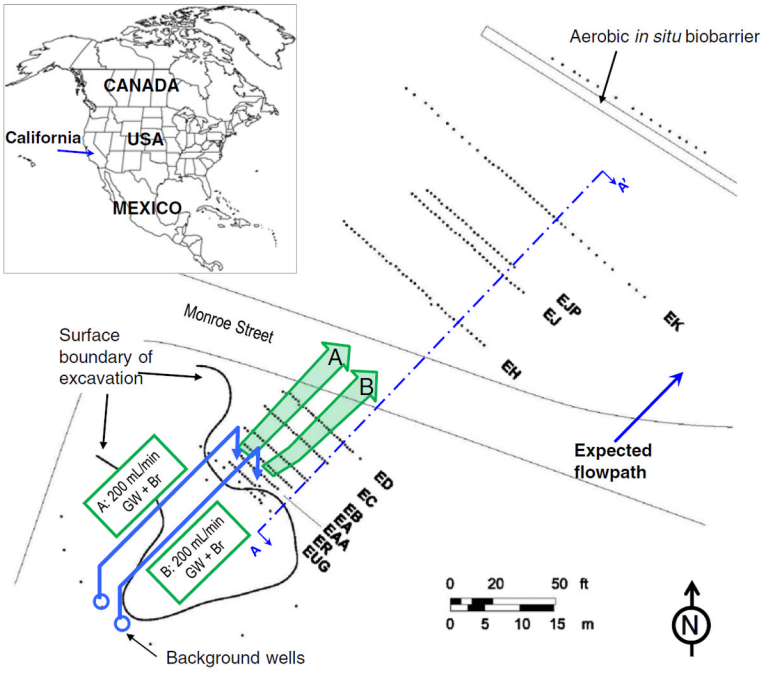

Fig. 1.

Map of site 60, Vandenberg Air Force Base (VAFB), California, showing the boundaries of the area excavated and backfilled in 1995 after the leaking underground storage tanks and piping were removed. The experimental layout and location of background groundwater supply wells, *EAA* injection wells, E-series monitoring wells (*EA*, *EB*, *EC*, *ED*, *EH*, *EJ* and *EJP*), and expected groundwater flow directions are illustrated. Tracer injection was intended to create two side-by-side bromide plumes (*colored arrows*) called lanes *A* and *B*. The vertical cross section *AA′* is presented in Fig. 2

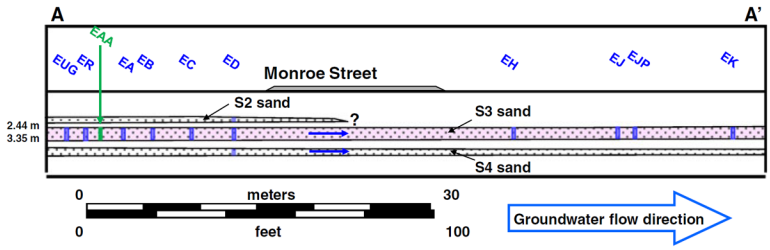

Fig. 2.

Vertical schematic illustrating the thin *S3* aquifer within which the experiment was conducted (section AA′ in Fig. 1), and the approximate locations of the transects of wells. The injection of bromide-spiked groundwater occurred in the *EAA* transect, as indicated by the *green arrow*

NIH-PA Author Manuscript NIH-PA Author Manuscript NIH-PA Author Manuscript

NIH-PA Author Manuscript

NIH-PA Author Manuscript

NIH-PA Author Manuscript

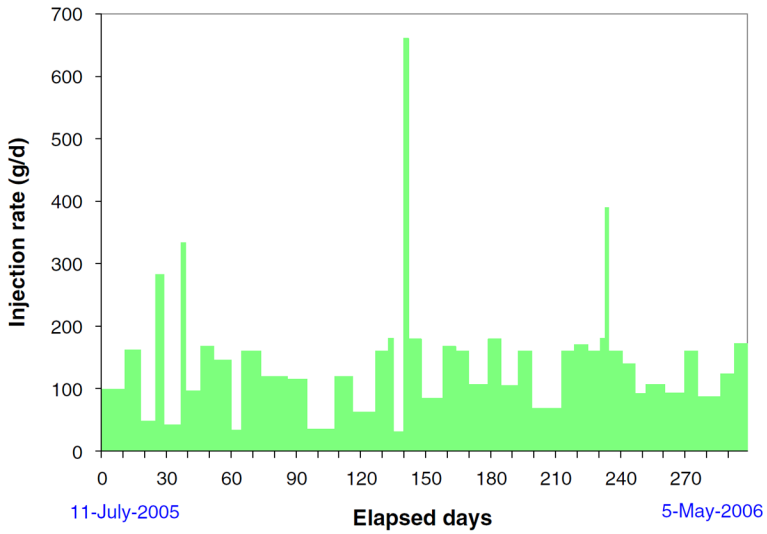

Fig. 3.

Bromide mass injection rates in grams per day (*g*/*d*). Instantaneous injection rates were calculated based on tracer reservoir volume and concentration measurement over time during the field experiment. This was used as the value for injected mass in the numerical model assuming a constant injection flow rate of 200 ml/d

NIH-PA Author Manuscript

NIH-PA Author Manuscript

NIH-PA Author Manuscript

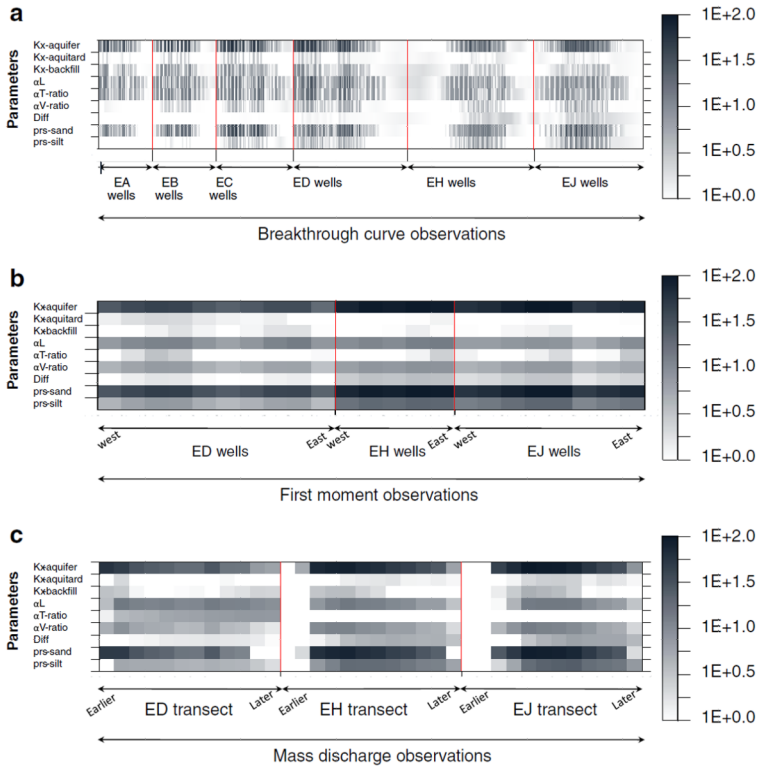

Fig. 4.

Dimensionless scaled sensitivity (DSS) plots (absolute values) for the model: **a** approach 1: with heads (133 observations) and concentrations (1,158 observations) in linear scale, **b** approach 2: with heads (133 observations) and temporal first moment of the breakthrough curves (23 observations) in linear scale, and **c** approach 3: with heads (133 observations) and tracer mass discharge (36 observations) in log scale. Each cell in the figure represents an observation data point in either space or time. Different groups of observations are highlighted and separated by *vertical red lines* to evaluate the impact of each group on the *parameters*

NIH-PA Author Manuscript

NIH-PA Author Manuscript

NIH-PA Author Manuscript

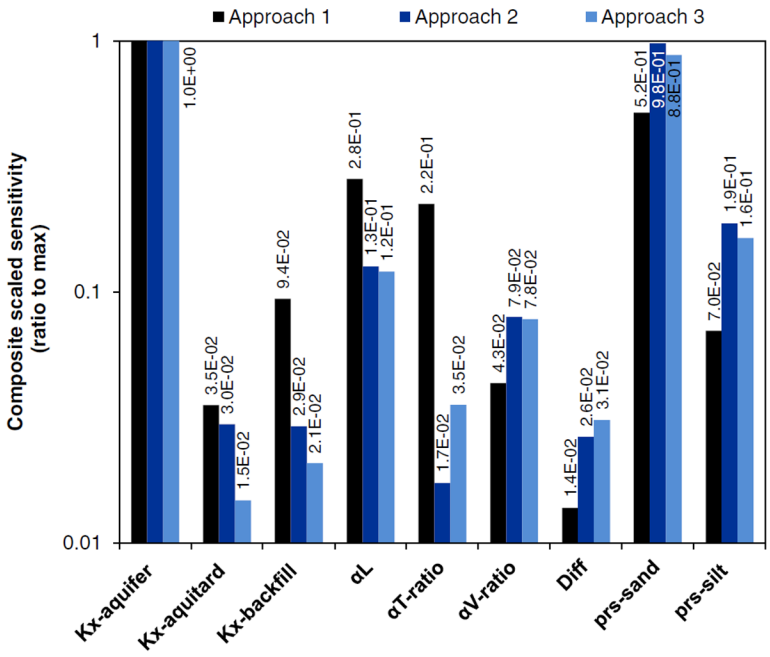

Fig. 5.

Composite scaled sensitivity (CSS) of model parameters (symbols defined in Table 1) in the three proposed approaches with three different sets of observations as noted in Table 2. Within each approach, CSS values are presented as the ratio to the maximum value. Sensitivity analysis was performed at the same initial parameter values (Table 1) for all three approaches. α*T-ratio* and α*V-ratio* represent the ratio of transverse horizontal and transverse vertical dispersivity to longitudinal dispersivity, respectively

NIH-PA Author Manuscript

NIH-PA Author Manuscript

NIH-PA Author Manuscript

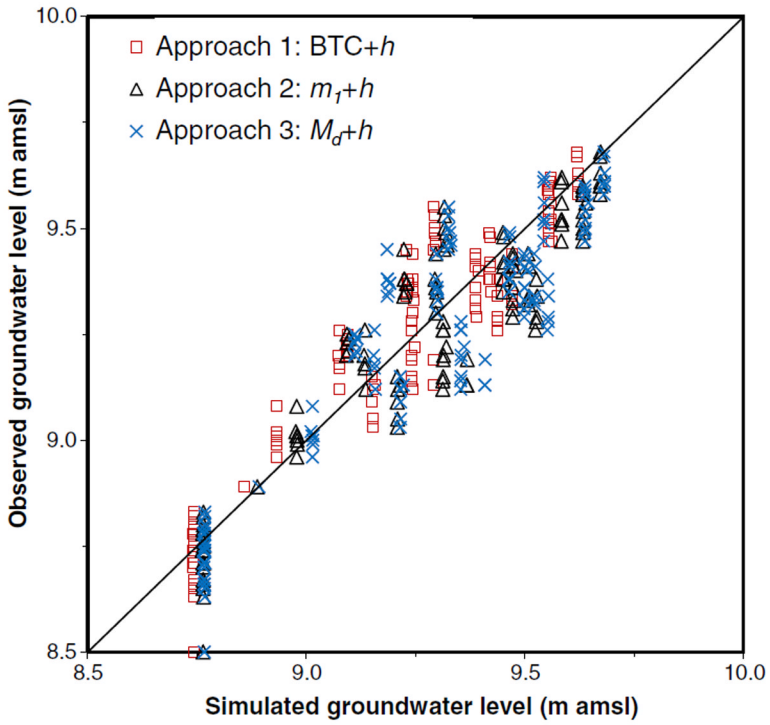

Fig. 6.

Comparing simulated versus observed values of hydraulic head in S3 aquifer for the three inverse modeling approaches proposed (i.e., *approach 1*: using hydraulic head combined with BTCs observations; *approach 2*: using hydraulic head combined with temporal first moment of breakthrough curve observations; *approach 3*: using hydraulic head combined with cumulative mass discharge observations). Units are meters above mean sea level

NIH-PA Author Manuscript
NIH-PA Author Manuscript
NIH-PA Author Manuscript

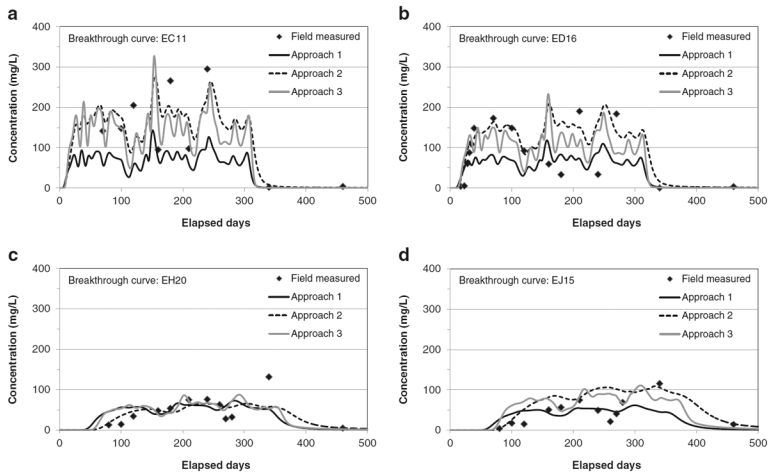

Fig. 7.

Comparison of observed versus simulated breakthrough curves for four arbitrarily chosen wells (*EC11*, *ED16*, *EH20*, and *EJ15*) from four different transects. Approaches 1–3 refer to the parameter estimation methods described in Table 2. Location of EC, ED, EH, and EJ wells are shown on Figs. 1 and 2

NIH-PA Author Manuscript
NIH-PA Author Manuscript
NIH-PA Author Manuscript

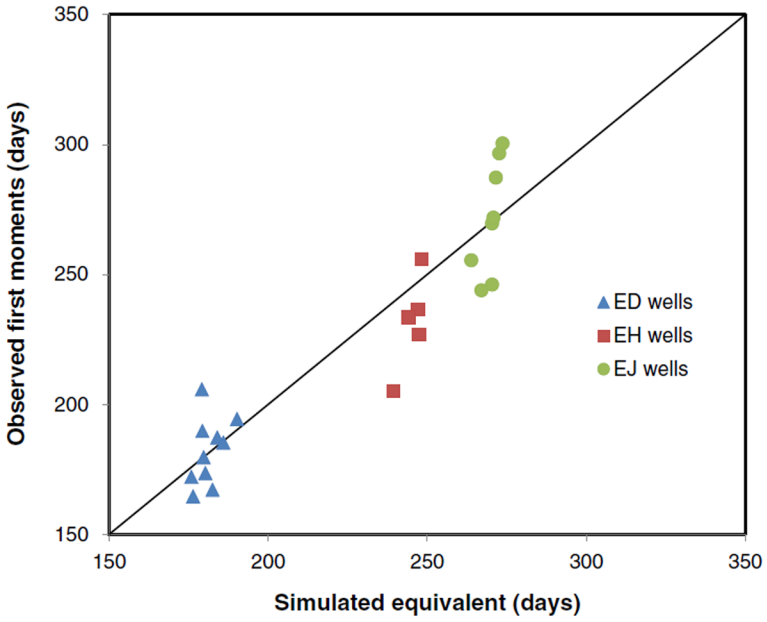

Fig. 8.

Observed versus simulated values of first moments of breakthrough curves after model calibration when head measurements and first moments of breakthrough curves were used to calibrate the model (approach 2). *ED*, *EH* and *EJ* are three monitoring well transects downgradient of the injection wells (Fig. 1) that were monitored over the course of this tracer experiment at VAFB

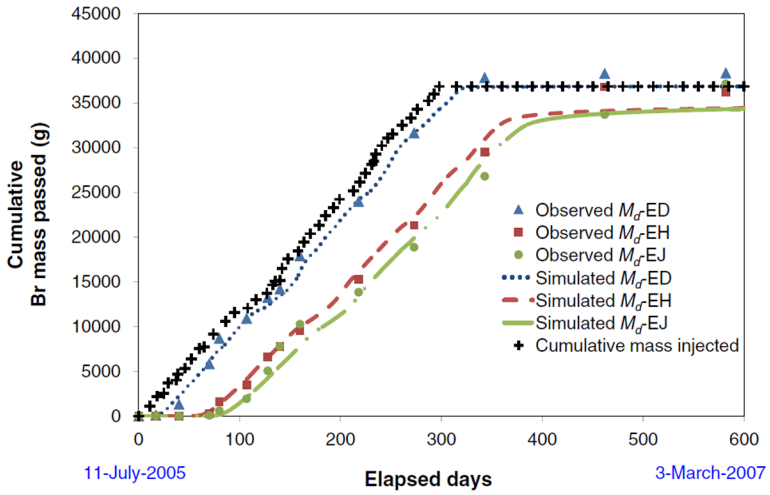

Fig. 9.

Observed versus simulated values of cumulative mass discharge through *ED*, *EH*, and *EJ* transects and comparison with the known tracer injected mass over time when the head measurements and mass discharge values were used for model calibration (approach 3)

NIH-PA Author Manuscript NIH-PA Author Manuscript NIH-PA Author Manuscript

NIH-PA Author Manuscript
NIH-PA Author Manuscript
NIH-PA Author Manuscript

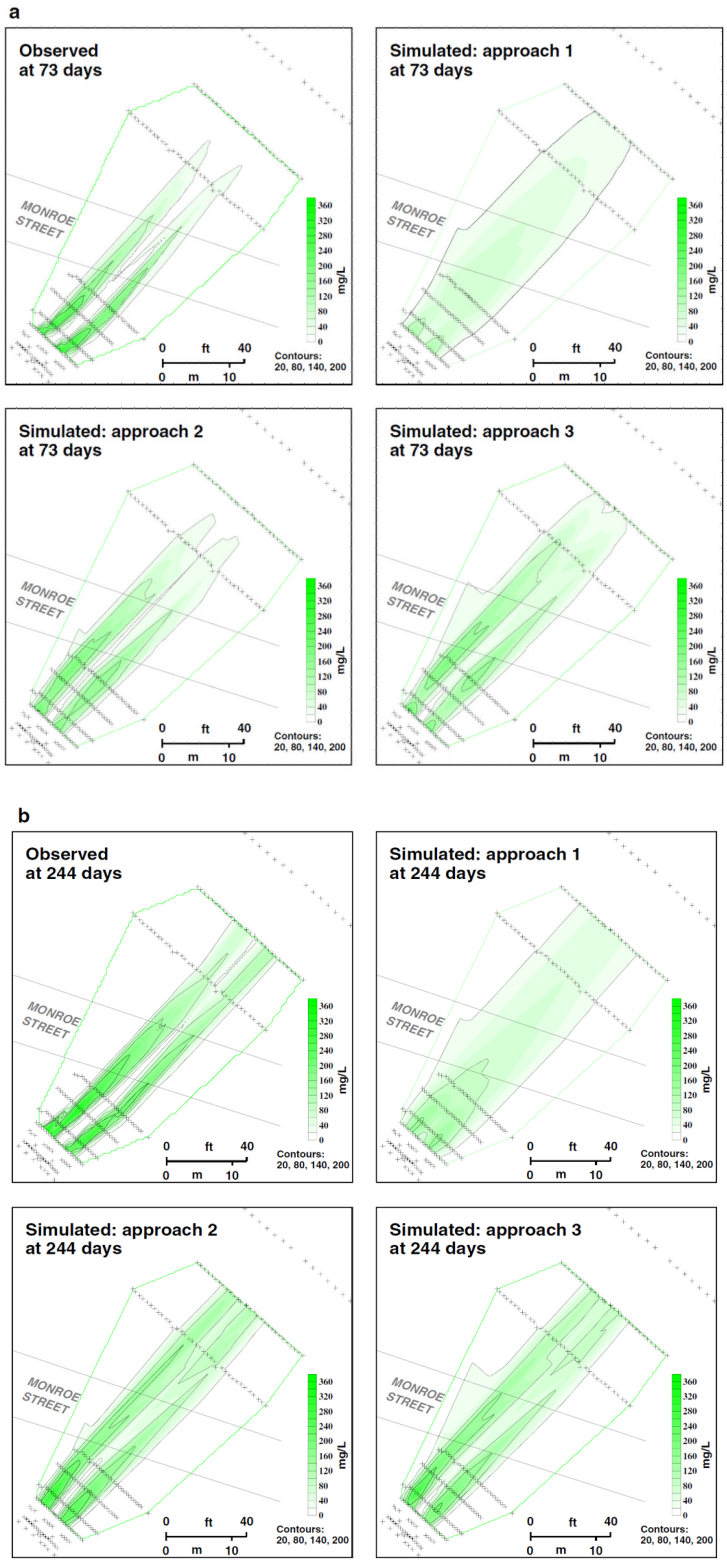

NIH-PA Author Manuscript

NIH-PA Author Manuscript

NIH-PA Author Manuscript

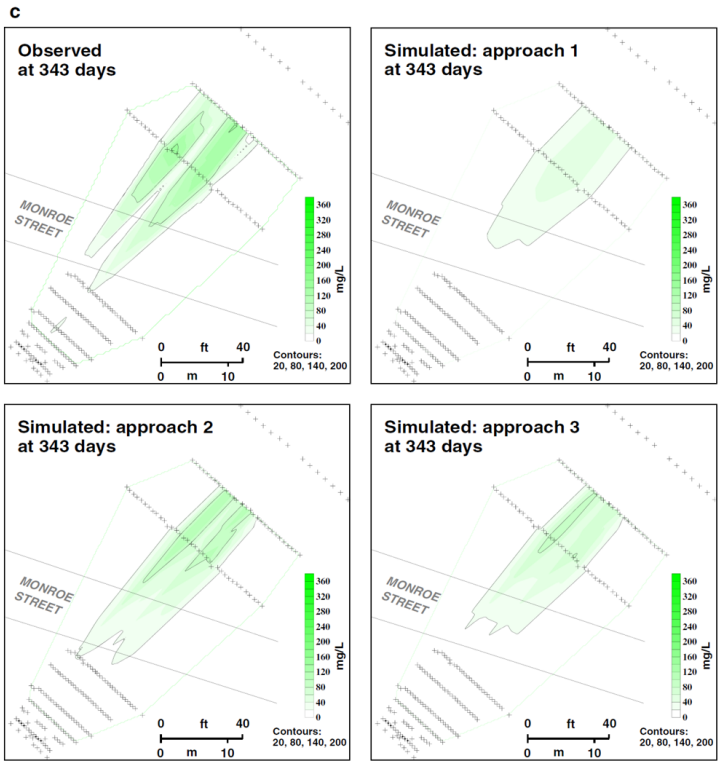

Fig. 10.

Comparison of the field observed versus simulated bromide tracer plume shapes based on the three calibration approaches at **a** 73 days, **b** 244 days, and **c** 344 days. Observed values correspond to plot based on the field observed bromide tracer data in mg/L; *approach 1* refers to using hydraulic head combined with BTCs observations; *approach 2* refers to using hydraulic head combined with temporal first moment of breakthrough curve observations; *approach 3* refers to using hydraulic head combined with cumulative mass discharge observations. *Contour lines* represent bromide concentration of 20, 80, 140, and 200 mg/L

NIH-PA Author Manuscript

NIH-PA Author Manuscript

NIH-PA Author Manuscript

Table 1

Model parameters. See text for discussion and assumed locations

Parameter (symbol, unit)	Initial value[a]	Source
Aquifer horizontal hydraulic conductivity($K_{x\text{-aquifer}}$, m/d)	13.7	(Mackay et al. 2012)
Silt layers horizontal hydraulic conductivity($K_{x\text{-aquitard}}$, m/d)	5×10^{-2}	(Rasa et al. 2011)
Backfilled zone horizontal hydraulic conductivity($K_{x\text{-backfill}}$, m/d)	45	Assumed
Horizontal to vertical hydraulic conductivity ratio (–)	10	Assumed
Hydraulic gradient (*i*, dimensionless)[b]	0.0132	(Mackay et al. 2012)
Aquifer total porosity (prs-sand, dimensionless)[b]	0.34	(Mackay et al. 2006)
Silt layers total porosity (prs-silt, dimensionless)[b]	0.4	(Rasa et al. 2011)
Retardation factor (*R*, dimensionless)[b]	1	Assumed
Longitudinal dispersivity (α_L, m)	0.5	(Rasa et al. 2011)
Transverse horizontal dispersivity (α_T, m)	0.05	(Rasa et al. 2011)
Transverse vertical dispersivity (α_V, m)[b]	5×10^{-3}	(Rasa et al. 2011)
Bromide aqueous diffusion coefficient (Diff, m^2/d)[b]	1.73×10^{-4}	(Mirkin et al. 1993; Patil et al. 1986)
Tortuosity (τ, dimensionless)[b]	0.4	(Parker et al. 2004; Rasa et al. 2011)

[a] Parameter values at the beginning of model development and before calibration or sensitivity analysis

[b] Value of this parameter was not calibrated and was kept constant during this study

NIH-PA Author Manuscript

NIH-PA Author Manuscript

NIH-PA Author Manuscript

Table 2

Observations included for each of the three different inverse modeling approaches

Observation type	Symbol	Number	Range	Weightingmethod[a]	Approach[b]		
					1	2	3
Hydraulic head(m amsl[c])	*h*	133	8.6–9.8	SD of 1.6 cm	Y	Y	Y
Breakthrough curve concentration (mg/L)	BTC	1158	0–350	CV of 0.1 for observations larger than 31 mg/L and SD of 3.1 mg/L for observations smaller than 31 mg/L	Y	N	N
Temporal first moment of BTC (days)	m1	23	150–350	Calculated based on the error associated with concentration measurements	N	Y	N
Cumulative mass discharge (g)	M_d	36	0–38352	Calculated based on the error associated with concentration measurements	N	N	Y

[a] *SD* means standard deviation. *CV* means coefficient of variations

[b] *Y* indicates the corresponding observation type was included in the approach. *N* means the observation type was not included in the approach

[c] Meters above mean sea level

NIH-PA Author Manuscript

NIH-PA Author Manuscript

NIH-PA Author Manuscript

Table 3

High (absolute value greater than 0.90) correlation coefficient between parameters (PCC). Parameter pairs with high PCC values were not included in the calibration model

Parameter[a]	Approach	α_T	α_V	Diff	prs-sand	prs-silt
α_L	1	0.95	-	-	-	-
	2	-[b]	-	-	-	-
	3	0.98	0.95	-	-	-
α_V	1	-	1.00	-	-	-
	2	-	1.00	0.99	0.99	0.99
	3	-	1.00	-	-	-
Diff	1	-	-	1.00	-	-
	2	-	0.99	1.00	0.99	0.99
	3	-	-	1.00	-	0.91
prs-sand	1	-	-	-	1.00	-
	2	-	0.99	0.99	1.00	1.00
	3	-	-	-	1.00	-

[a] Table rows with no high PCC value are removed

[b] The dash (-) represents absolute PCC values less than 0.90

NIH-PA Author Manuscript

NIH-PA Author Manuscript

NIH-PA Author Manuscript

Table 4

Inverse modeling parameters and their final values for the three proposed approaches

Parameter	Optimized parameter values and95 % confidence interval		
	Approach 1: BTC+/*h*	**Approach 2: m_1+*h***	**Approach 3: M_d+*h***
$K_{x\text{-aquifer}}$ (m/d)	16.96(15.11, 19.02)[a]	10.89(9.97, 11.90)	12.64(11.59, 13.78)
$K_{x\text{-quitard}}$ (m/d)	0.18(4.5×10^{-2}, 0.72)	1.7×10^{-2}(2.6×10^{-3}, 1.0×1.0^{-1})	$5.5\times l0^{-4}$($2.4\times l0^{-6}$, 1.3×10^{-1})
$K_{x\text{-backfill}}$ (m/d)	4.63(0.82, 26.03)	120.3(46.2, 313.0)	1,843.0(122.9, 27647.9)
α_L (m)	0.40(0.25, 0.63)	0.55(0.34, 0.88)	0.18(0.09, 0.37)
α_T (m)	0.15(0.11, 0.21)	0.01(7.6×10^{-3}, 0.02)	0.05[b]

[a] Intervals in *parentheses* indicate the 95 % confidence interval of the calibrated parameter

[b] Transverse horizontal dispersivity (α_T) was not calibrated in the third approach due to its high correlation with longitudinal dispersivity parameters (as discussed in the text and Table 3)